ADVANCED OPTICAL MATERIALS
www.advopticalmat.de

Polarization-Controlled Chromo-Encryption

*Hsiang-Chu Wang and Olivier J. F. Martin**

The response of simple plasmonic nanorods to polarized illumination is studied in detail. Depending on the orientation of that polarization with respect to the symmetry axes of the nanostructure, a chiral response can occur, which can be analyzed through a second polarizer, in order to control the spectral response of the system. Specifically, for the Ag nanorods fabricated here, a broad variety of colors can be produced that cover half of the chromaticity diagram. Depending on the illumination and detection polarizations, these colors range from white to vivid colors or even black, in spite of the fact that the material at hand does not absorb much light. By exploiting two additional degrees of freedom, namely the nanorod length and its orientation within the unit cell, it is possible to produce a very rich palette of optical effects that are controlled by the polarization of light. Their utilization to reproduce artworks is demonstrated, together with their operation as encrypting system, where the polarizations are used as keys and the message is encrypted in a quaternary color subset.

1. Introduction

Structural colors,[1] with their stability, environmental friendliness, and extremely high spatial resolution, enable applications in passive colors for decoration, displays,[2] high-density optical storage,[3] information processing,[4] and encryption.[5] Different types of structures have been demonstrated for those applications, including groves,[6] gratings,[7] films,[8] apertures, nanoparticles,[9] and related structures.[10] In order to increase the information density the variation of the optical response under different polarization states has also been used with geometries such as rectangles,[11] crosses,[12] and ellipses.[13]

Optical cryptography involves recording or transmission of concealed information by means of light where only the employment of correct keys enables the interpretation of the original information. Conventional methods, in general, utilize a phase key to encrypt the original information and a corresponding phase key to decrypt the encrypted information.[14] This concept has been adopted in meta-holograms by illuminating a metasurface (encrypted information) with a modulated incident light (key).[15] Another group has patterned the encrypted information by encoding the orbital angular momentum helical phase and Fourier transform lens, such that when decrypting with correct keys (time-dependent incident beams) the encrypted information becomes comprehensive.[16] In addition to reconstructing the information in the far field like holograms, encrypted metasurfaces composed of complex-amplitude units can be arranged into gray scale or color images.[17] Combining the channels in the far field and near field makes optical encryption more versatile, like in binary or color QR codes.[18] Since the spectral response of nanostructures is generally sensitive to the polarization orientation it can serve as key to decrypt information.[19] However, these encryption concepts are not yet utilized to their full potential. In this work, we use a simple geometry to demonstrate a plethora of spectral responses, which are then employed for encryption using a quaternary system.

Here, we resort to silver (Ag) for its low losses in the visible.[20] Each color pixel (unit cell) contains a rectangular Ag nanorod on a dielectric pedestal that forms an aperture of similar geometry within an Ag mirror underneath (see Experimental Section). The unit cells are placed on a square array with period 300 nm, which prevents grating diffraction orders and Wood-Rayleigh anomalies at the visible wavelengths of interest.[21] The coupling between the nanostructures and the mirror plane is negligible since the pedestal height is larger than 80 nm.[22] The readout scheme is illustrated in **Figure 1**a, incident light (in black), passing through a linear polarizer and a polarization insensitive beam splitter, impinges on the sample. The reflected light (in red) is then analyzed with another polarizer (analyzer). When both polarizers are parallel with the nanostructures (horizontal, H-direction, Figure 1b), the observed colors are muted, with a low chroma caused by the low Ag absorption. When rotating both polarizers perpendicular to the nanostructures (vertical, V-direction, Figure 1c), all the colors appear grey due to the lack of dimensional variations in this direction. However, the colors become vivid and saturated when both polarizers are in the diagonal direction (+45°, D-direction), Figure 1d. This difference of color contrast controlled by the mere orientation of the polarization is quite baffling, since it contradicts our intuition that the response for diagonal polarization could be inferred from the superposition

H.-C. Wang, O. J. F. Martin
Nanophotonics and Metrology Laboratory
Swiss Federal Institute of Technology Lausanne (EPFL)
Lausanne 1015, Switzerland
E-mail: olivier.martin@epfl.ch

The ORCID identification number(s) for the author(s) of this article can be found under https://doi.org/10.1002/adom.202202165.

DOI: 10.1002/adom.202202165

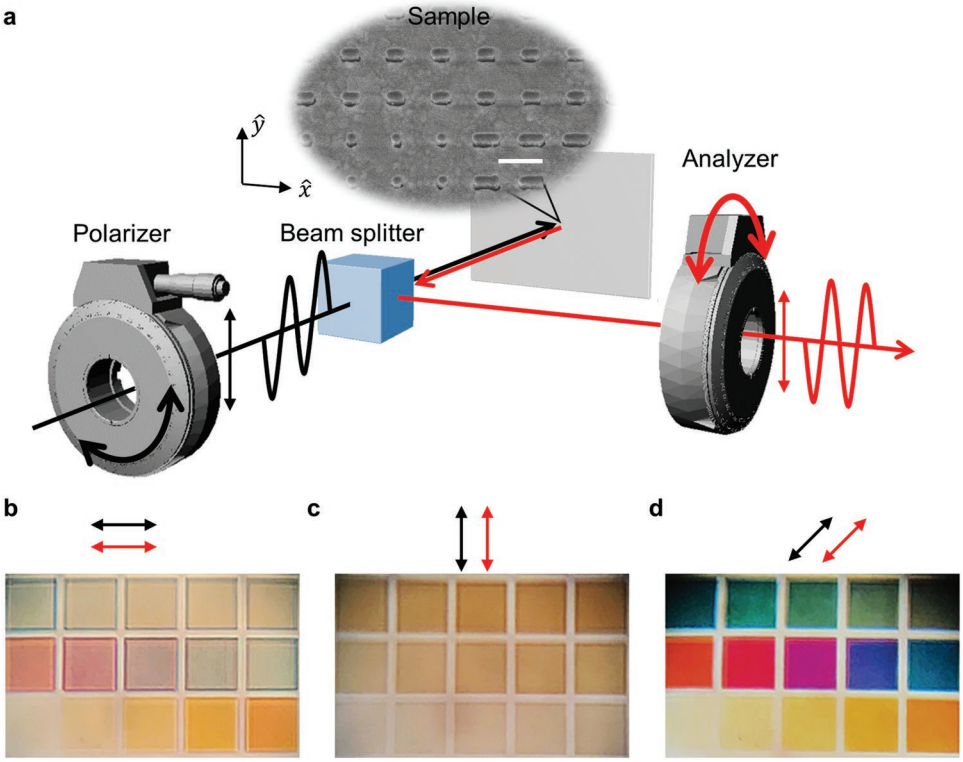

Figure 1. Color contrast controlled by polarization. a) Readout principle: each color pixel contains a rectangular Ag nanostructure (scale bar 300 nm). The incident polarization is controlled with a polarizer and the scattered light goes through another polarizer (analyzer). b) Muted colors with low chroma are generated when the polarizer and analyzer are parallel to the nanostructures axis (horizontal polarization). c) When rotating both polarizers perpendicular to the nanostructures axis, all the colors appear greyish (vertical polarization). d) When both polarizers are rotated by 45°, along the diagonal direction, vivid and saturated colors are observed.

of the responses for H- and V-directions. There is however a flaw in that simple application of the principle of superposition, as explained next. The strong dependence of the color contrast on polarization observed in Figure 1 forms the foundation for the chromo-encryption presented here.

2. Principle of Superposition and Polarization-Induced Chirality

The principle of superposition, which stems from the linearity of Maxwell's equations, is ubiquitous in photonics, to the extent that it can pervert our intuition. For example, one would intuitively assume that the optical response of an optical system under diagonal illumination can be inferred from the combined responses for horizontal and vertical illuminations. However, the bleak colors observed under horizontal polarization (H-direction, Figure 1b) or vertical polarization (V-direction, Figure 1c) are turning vivid under diagonal polarization (+45°, D-direction, Figure 1d). This implies that the reflected light intensity under diagonal illumination cannot be deduced from the mere superposition of those along H- and V-directions by applying the principle of superposition naively. As a matter of fact, the principle of superposition cannot be applied to the intensity of light, but is only valid for its amplitude. It is however possible to make a link between the light detected diagonally and the horizontal and vertical components of the illumination field by introducing E_β^α for the electric field amplitude reflected from the sample, where α indicates the polarization of the incident field and β the polarization of the reflected light. The reflected intensity measured under unit amplitude diagonal polarization can then be written as

$$R^{\mathrm{D}} = \left|\left(E_{\mathrm{H}}^{\mathrm{H}} + E_H^V\right)\hat{h} + \left(E_{\mathrm{V}}^{\mathrm{V}} + E_{\mathrm{V}}^{\mathrm{H}}\right)\hat{v}\right|^2 = \left[\left(E_{\mathrm{H}}^{\mathrm{H}} + E_{\mathrm{H}}^{\mathrm{V}}\right)^2 + \left(E_{\mathrm{V}}^{\mathrm{V}} + E_{\mathrm{V}}^{\mathrm{H}}\right)^2\right] = \left[\left(E_{\mathrm{H}}^{\mathrm{H}}\right)^2 + 2E_{\mathrm{H}}^{\mathrm{H}}E_{\mathrm{H}}^{\mathrm{V}} + \left(E_{\mathrm{H}}^{\mathrm{V}}\right)^2 + \left(E_{\mathrm{V}}^{\mathrm{V}}\right)^2 + 2E_{\mathrm{V}}^{\mathrm{V}}E_{\mathrm{V}}^{\mathrm{H}} + \left(E_{\mathrm{V}}^{\mathrm{H}}\right)^2\right] \quad (1.1)$$

where $\hat{h}$ and $\hat{v}$ are unit vectors along the horizontal and vertical directions. Obviously, this intensity is different from the sum of those reflected at 0° and 90°

$$R^{\mathrm{D}} \neq R^{\mathrm{H}} + R^{\mathrm{V}} = \left[\left(E_{\mathrm{H}}^{\mathrm{H}}\right)^2 + \left(E_{\mathrm{V}}^{\mathrm{V}}\right)^2\right] \quad (1.2)$$

Except for the very special case when all cross polarization terms vanish: $E_{\mathrm{H}}^{\mathrm{V}} = E_{\mathrm{V}}^{\mathrm{H}} = 0$ (see Section S1, Supporting Information). This condition occurs very rarely; it would for example be the case for a perfectly cylindrical scatterer. For most structures, including the nanorod pixel considered here, the response is always anisotropic or chiral, meaning that the cross-polarization terms do not vanish and the optical response under diagonal polarization can be very different from that under horizontal or vertical polarizations, as visible in Figure 1b–d.

It might be surprising that a very simple structure with two mirror symmetry planes like the nanorod considered here

exhibits chirality. In the scientific literature, quite complicated structures, like the gammadion represent the archetype of a chiral structure.[23] However, as described in details by Okamoto,[24] a nanorod exhibits chirality as soon as it is illuminated with light polarized different from one of its symmetry axes (H- or V-directions in the case of Figure 1).

3. Results

3.1. Polarization Controls Colors

Let us first study numerically the cross-polarization terms for the unit cell depicted in **Figure 2**a using full-wave simulations with periodic boundary conditions. Such a structure is easy to achieve by two-step fabrication (see Experimental Section). The only variable is the length L of the rectangular structures; the simulated and measured reflectance spectra for L between 40 and 200 nm are presented in Section S2, Supporting Information. As an example, let us discuss the sample with $L = 100$ nm: the tilted SEM image of a typical Ag rectangular array is displayed in Figure 2b. The simulated spectra for reflectance and phase shift are plotted in Figure 2c. To study the effect of the illumination and detection polarizations, we introduce a similar notation as in Section 2 for the reflectance: R^{α}_{β}, where α indicates the polarization of the incident field (polarizer in Figure 1a) and β that of the reflected field (analyzer in Figure 1a). When both polarizations are collinear the reflectance is not strongly modulated, see $R^{\mathrm{H}}_{\mathrm{H}}$ and $R^{\mathrm{V}}_{\mathrm{V}}$ in Figure 2c, leading to the muted colors visible in Figure 1b,c. For cross polarizations, $R^{\mathrm{V}}_{\mathrm{H}}$ and $R^{\mathrm{H}}_{\mathrm{V}}$, the reflectance is so small that it cannot be shown in Figure 2c and the structures appear black. On the other hand, vivid colors are observed in Figure 1d under diagonal illumination and detection. The reason for this effect can be understood by studying the corresponding phase shift and reflectance spectra under H- and V-polarized illumination in Figure 2d. The spectrum under diagonal polarized illumination $R^{\mathrm{D}}_{\mathrm{D}}$ is drawn in brown; it has the deepest trough among the different polarizations investigated, indicative of the strongest color. Since Ag is a low loss plasmonic material, it is hard to explain this deep trough with absorption.[25] On the other hand, the phase shift associated with the reflectance provides a clue on the phenomenon. The three purple arrows in Figure 2c and d indicate the spectral locations where the phase shift differences τ between $R^{\mathrm{H}}_{\mathrm{H}}$ and $R^{\mathrm{V}}_{\mathrm{V}}$, defined as $\tau = \Phi^{\mathrm{H}}_{\mathrm{H}} - \Phi^{\mathrm{V}}_{\mathrm{V}}$, amount to +90°, 180°, and −90°, respectively (from left to right). These values correspond to special polarizations, namely right circular (R), anti-diagonal (A), and left circular (L) polarization states, respectively. In fact, the phase shift difference τ determines the conversion of polarization states. The polarization states can be easily interpreted through the observation of the electric fields that oscillate with time. The oscillation patterns for different polarization states are presented in Section S3, Supporting Information. The plot in Figure 2d describes how the incident light is converted by the unit cell under diagonal polarization illumination into a color spectrum. The incident light (black arrow) can be decomposed into $E^{\mathrm{H}}_{\mathrm{inc}}$ and $E^{\mathrm{V}}_{\mathrm{inc}}$. When reflected, the phase shift transforms the incident light $E^{\mathrm{H}}_{\mathrm{inc}}$ into $E^{\alpha}_{\mathrm{ref}}$ with a different polarization state α: for a phase shift difference of 180°, the unit cell acts as a half-wave plate, while for a phase shift difference of ±90°, it acts as a quarter-wave plate. The corresponding spectra are simulated in Figure 2e. A maximum cross-polarization peak is detected for $\tau = 180°$, leading to the trough in $R^{\mathrm{D}}_{\mathrm{D}}$. The extreme for right and left circular polarizations are at the intersections of the $R^{\mathrm{D}}_{\mathrm{D}}$ (in brown) and $R^{\mathrm{D}}_{\mathrm{A}}$ (in grey green), where the phase shifts are ±90°. The corresponding reflectances measured for $R^{\mathrm{H}}_{\mathrm{H}}$, $R^{\mathrm{V}}_{\mathrm{V}}$, $R^{\mathrm{D}}_{\mathrm{D}}$, $R^{\mathrm{D}}_{\mathrm{A}}$, $R^{\mathrm{D}}_{\mathrm{R}}$, and $R^{\mathrm{D}}_{\mathrm{L}}$ are shown in Figure 2f. In Figure S1, Supporting Information, the trough in the spectrum red shifts with increasing lengths L, which generates rainbow colors by changing L. For the cross-polarization spectra $R^{\mathrm{D}}_{\mathrm{A}}$, the colors are complimentary to the colors of the co-polarization spectra $R^{\mathrm{D}}_{\mathrm{D}}$. Likewise, the colors of $R^{\mathrm{D}}_{\mathrm{R}}$ are also complimentary to those of $R^{\mathrm{D}}_{\mathrm{L}}$.

Since the structure exhibits a different response to the polarization throughout the entire visible range, the spectral response varies with the polarization used. This is illustrated in **Figure 3**, where we consider nanostructures of varying lengths L between 40 and 200 nm. Six different polarization states (H, V, D, A, R, L) and their most interesting combinations are considered for illumination and detection, Figure 3a. These spectra correspond to different colors, as illustrated in Figure 3b–d with the Commission internationale de l'éclairage (CIE 1931) diagrams.[26] For example, Figure 3b shows the different colors when illuminating with H-polarized light, and detecting with H, D, A, R, and L: all these colors are muted, centered around the CIE map region with coordinates x and y between 0.3 and 0.4. As for the cross polarization terms $R^{\mathrm{H}}_{\mathrm{V}}$, denoted as green crosses, they are black due to no contributions into this polarization state (like $R^{\mathrm{H}}_{\mathrm{V}}$ curve in Figure 2c). Note that the CIE chromaticity diagram does not include the brightness information. A similar behavior is observed for illumination with V-polarized light shown in Figure 2c ($R^{\mathrm{V}}_{\mathrm{H}}$ curve). On the contrary, illuminating these horizontally aligned structures with polarization states such as D, A, R, and L can dramatically expand the detected colors, as evident in Figure 3c for D-polarized illumination and in Figure 3d for R-polarized illumination. Additional illumination polarizations are shown in Section S4, Supporting Information. In any case, colors illuminated along the symmetry axes of these rectangular structures, that is, with H- or V-polarizations, remain muted. Other geometries could of course unmute these colors and achieve similar possibilities. For the nanorod shapes studied here, although the colors are muted and not very vivid, the human eyes can still notice their subtle differences, as shown in Figure 1b.

Based on the idea that colors of nanorods with only one variable L cover broad area on a CIE map, we can utilize these different polarization-controlled colors to reproduce the oil painting "Mediterranean Landscape" by Pablo Picasso (copyright Succession Picasso/2022, ProLitteris, Zurich). The original is reproduced in **Figure 4**a. Pixels on the painting are replaced by nanorods with different lengths aligned horizontally. Using the same two-step process of first patterning HSQ with electron beam lithography and then depositing Ag, we obtain a nano-painting (360 μm × 235 μm). Under electron scanning microscope, this nano-painting exhibits a grey scale before (Figure 4b) and after (Figure 4c) Ag deposition. Under polarized white light illumination, it presents different colors depending on the illumination and detection polarizations.

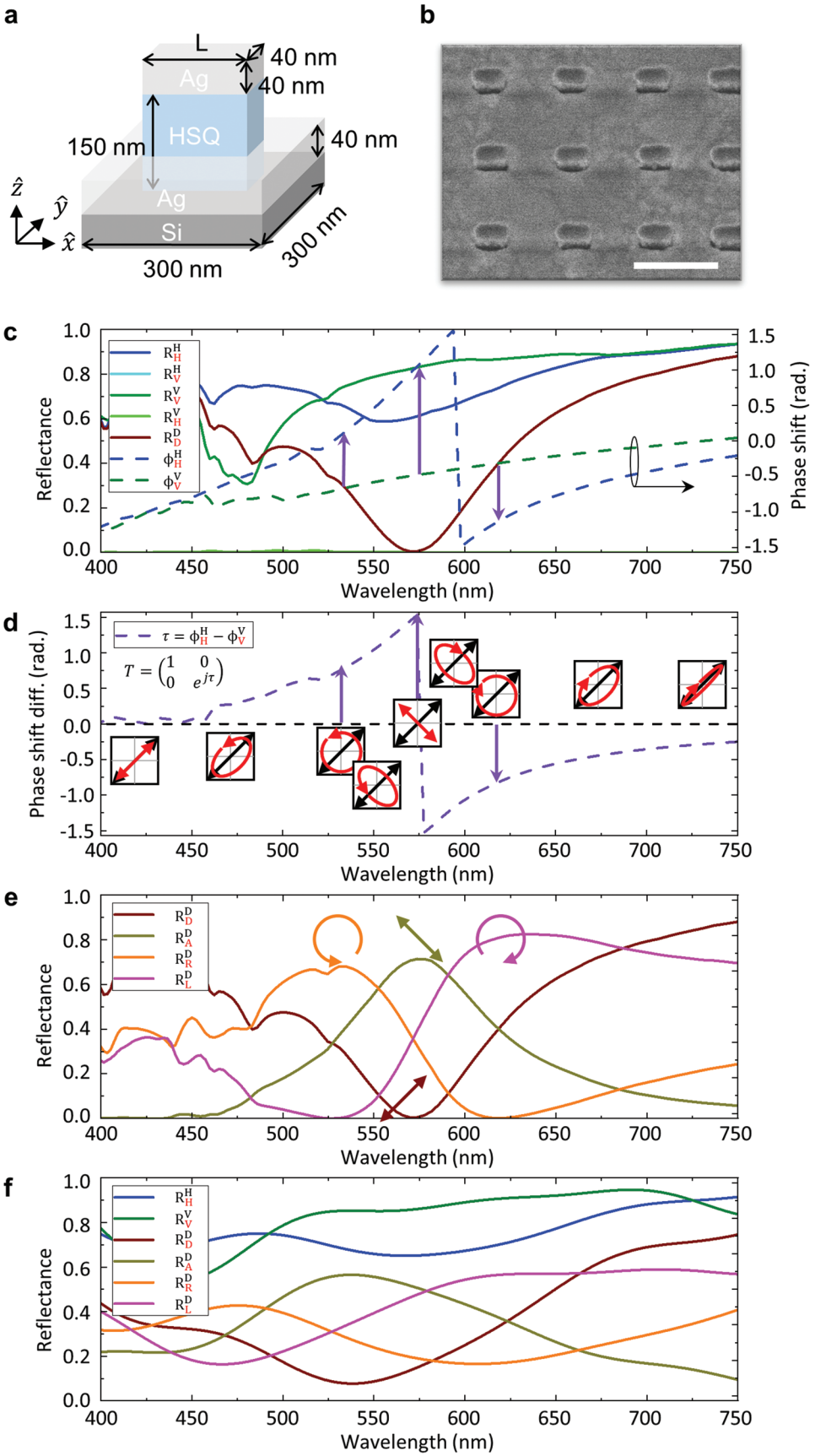

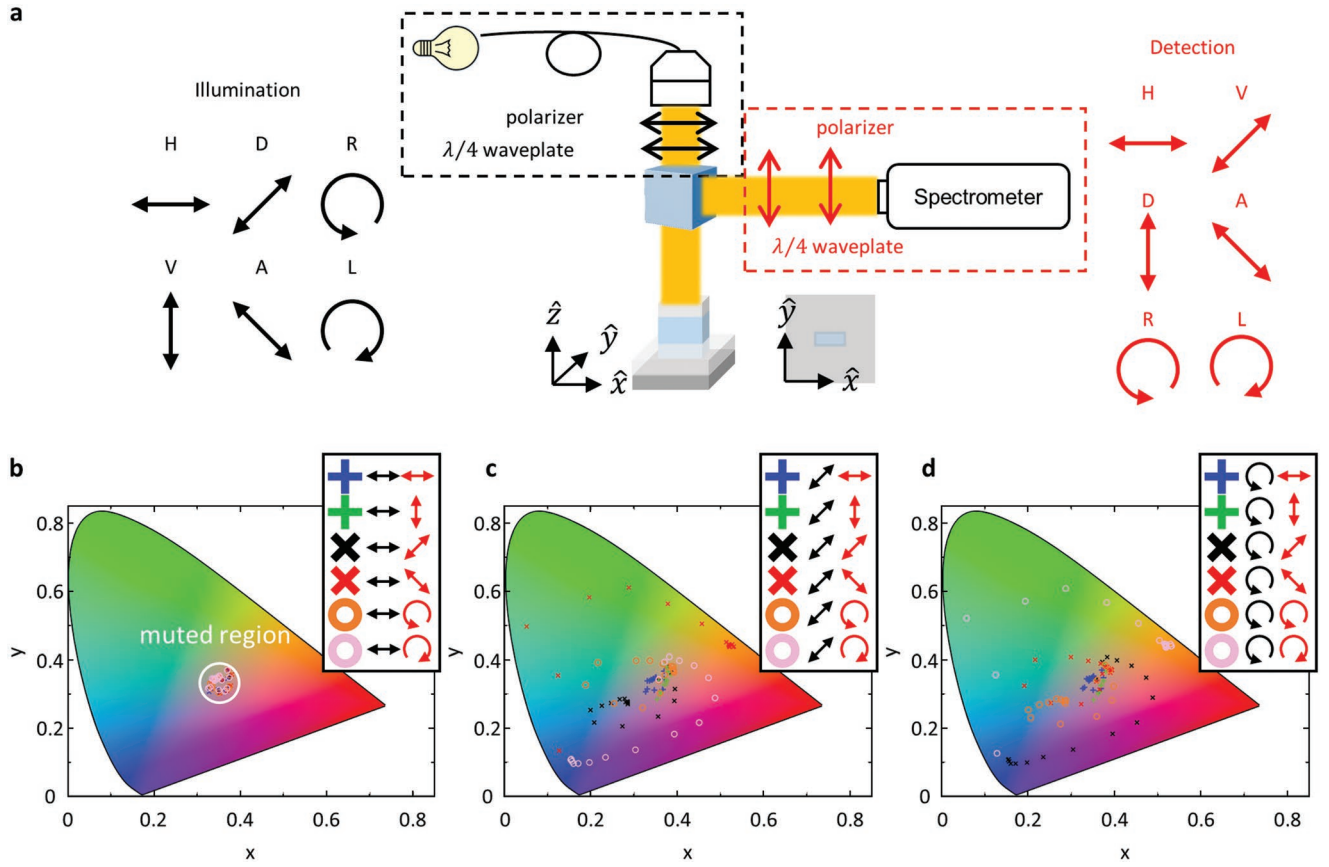

Figure 3. Reflectance color space covered by changing the nanorod length between L = 40 and 200 nm for different polarization combinations. a) Polarizations used for illumination and detection. b) Horizontal illumination polarization produces muted colors that accumulate in the center of the CIE chromaticity diagram. c) Diagonal illumination polarization produces vivid colors that cover half of the chromaticity diagram. d) Right circular illumination polarization produces similar effects with different colors.

(The minor color differences between Figure 4a and e is mainly caused by the color quantization described in Figure S9, Supporting Information; in addition some nanofabrication inaccuracies as well as the camera used to take the image in Figure 4e contribute to those color differences). For example, illuminated and detected with both H-polarizations (Figure 4d) or both V-polarizations (Figure 4g), as expected the colors of the nano-painting are muted, Figure 3b. To unmute the colors of these horizontal rods, the polarizations of illumination must differ from H- or V-directions, which is simulated in Figure 3c and d. In this demonstration, the correct color will be displayed by illuminating and detecting in D-direction $R_{\mathrm{D}}^{\mathrm{D}}$ as shown in Figure 4e, where a color quantized image quite close to the original is recovered. A finer nano-painting can be achieved by applying additional quantized colors.[27] The details for the color quantization are presented in Section S5, Supporting Information. This demonstrated nano-painting utilizes only 9 different rods, including black color. When observed with other polarization pairs such as $R_{\mathrm{R}}^{\mathrm{D}}$ in Figure 4f, $R_{\mathrm{A}}^{\mathrm{D}}$ in Figure 4h, or $R_{\mathrm{L}}^{\mathrm{D}}$ in Figure 4i, other colors are displayed. Let us consider the red building as an example: the wall is designed in red; this color is muted under $R_{\mathrm{H}}^{\mathrm{H}}$ (Figure 4d) and turns grey under $R_{\mathrm{V}}^{\mathrm{V}}$ (Figure 4g). On the other hand, it becomes a strong and saturated red under $R_{\mathrm{D}}^{\mathrm{D}}$, and switches to the complimentary color—cyan—under $R_{\mathrm{A}}^{\mathrm{D}}$, Figure 4h. When detected with R- or L-polarization, the colors are either blue-shifted or red-shifted. It might appear counterintuitive to achieve black by addition of primary colors, whose mixture normally turns white. Actually, here the black color is achieved by converting the D-polarized incident light into A-polarized light, since the structure of interest has very limited absorption. That is why the dark areas in Figure 4e appear bright in Figure 4h. The approach of mixing colors to achieve brighter or darker rainbow colors is to add black or white unit cells into a pixel array, as described in

Figure 2. Colors controlled by the illumination and detection polarizations. a) Unit cell used in this work, with the nanorod aligned horizontally. b) Titled SEM image of a typical fabricated sample, scale bar 300 nm. c) Computed reflectances R_{β}^{α} and phases Φ_{β}^{α} for different combinations of the illumination polarization α and the detection polarization β. Phase shift between the incident and the reflected lights, induced by the sample (see text for details). d) Polarization states of reflected light (red arrows) as a function τ under diagonal polarization illumination (black arrows). e) Computed reflectances for diagonal polarized illumination and four different detection polarizations. f) Measured reflectance for the sample in (b) for different polarization combinations. Panels (c)–(f) are for L = 100 nm.

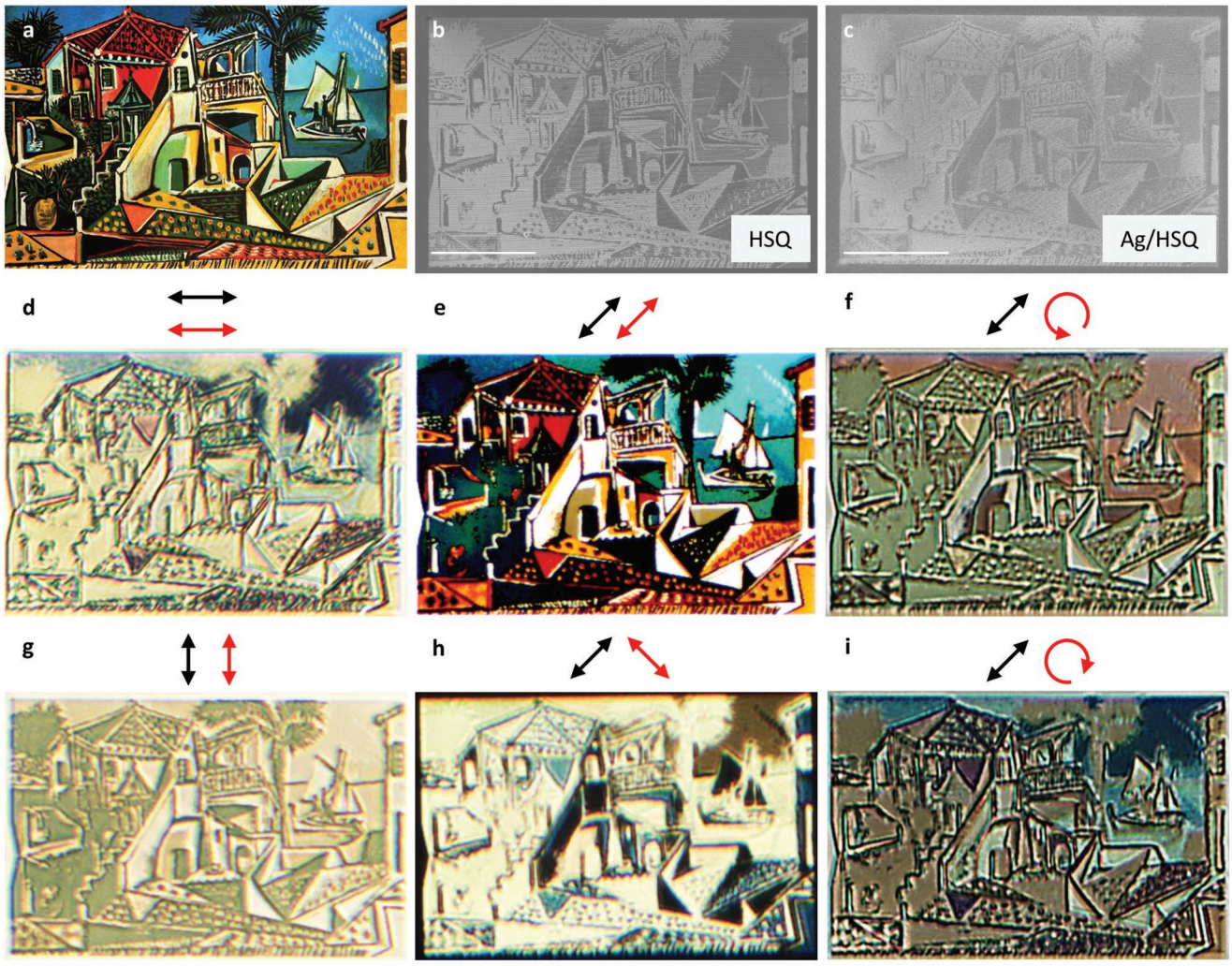

Figure 4. Nano-printing of the "Mediterranean Landscape" by Pablo Picasso. a) Original painting (reproduced with permission, copyright Succession Picasso/2022, ProLitteris, Zurich). SEM images of the sample b) before and c) after Ag deposition. Bright field microscope images for different illumination–detection polarization pairs: d) horizontal–horizontal; e) diagonal–diagonal; f) diagonal–RCP; g) vertical–vertical; h) diagonal–anti-diagonal; i) diagonal–LCP.

Section S6, Supporting Information. Hence, black is composed of two nanorod units, while white is composed of shorter rods with length 60 nm. A pure color such as red is composed of a single length rod in a unit cell. The brighter blue is a mixture of blue and white units: by adding the black and white units into the pure single rod color, we are able to tune the brightness of the rainbow colors (see SEM images in Section S7, Supporting Information).

3.2. Chromo-Encryption

Now that we have established that the color exhibited by a simple nanorod depends on the illumination and detection polarizations, this optical property can serve as basis for encryption with structural colors. The connection between structural colors and keys in encryption applications is demonstrated in **Figure 5**, where the illumination–detection polarization pair represents a key for that encryption system. Although the palette at hand could also support the octal system under proper definitions, we use the quaternary number system[28] for simplicity. In this system, the plain text "Hello!" will be translated into a series of digits 0, 1, 2, and 3. Letters and symbols are defined in ASCII with the binary code that is directly converted it into quaternary digits, 1020 1211 1230 1230 0201 in this example, Figure 5a. These digits are later defined on a table of structural colors.

So far, we have focused on nanorods oriented in H-direction only; to increase the utility of keys, we also now include four orientation angles (<1: 0°, <2: 45°, <3: 90°, and <4: 135°). The corresponding colors for different illumination and the detection polarizations are exhibited in the tables shown in Section S8, Supporting Information. One can notice that the colors are hopping between keys as nanorods rotate. Assuming that only linear polarization states (H, V, D, and A) are used for illumination, while detection polarizations can be

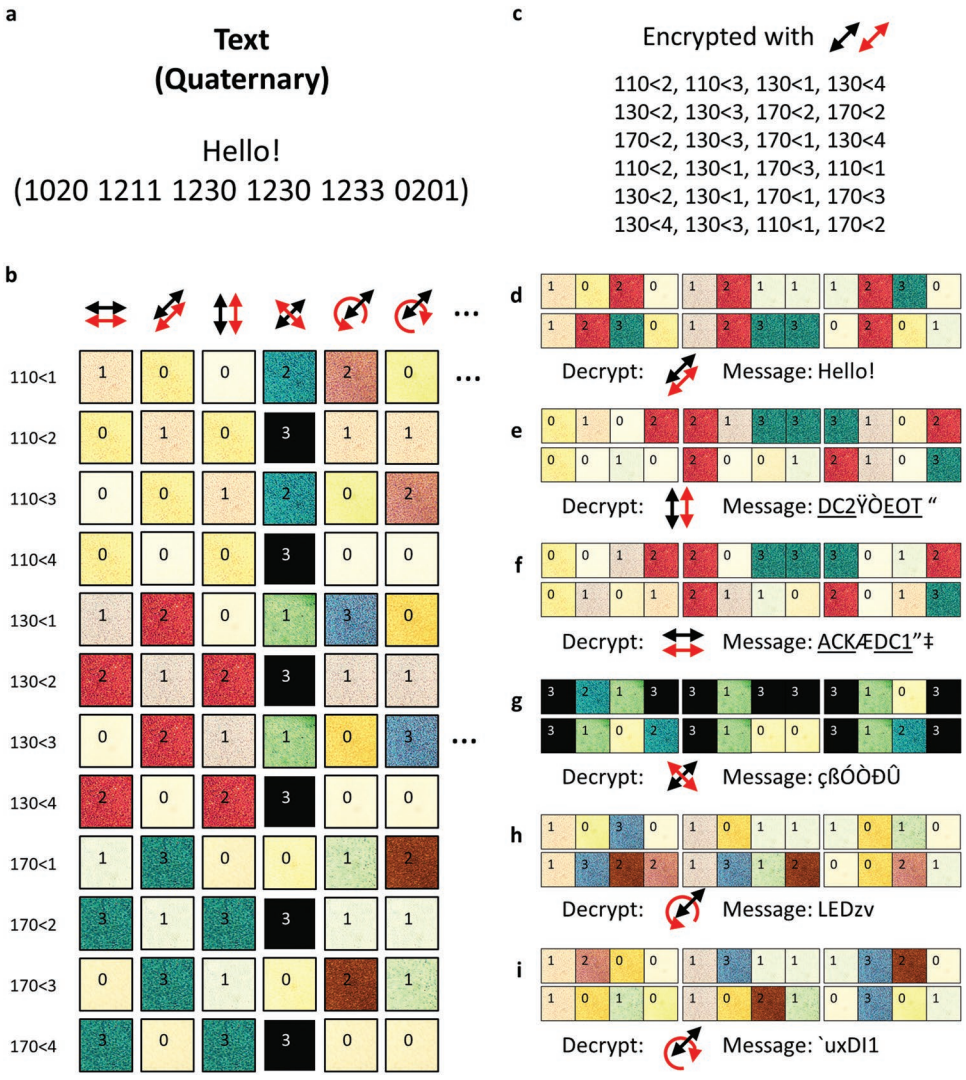

Figure 5. Polarization-controlled chromo-encryption. a) The secret message “Hello!” is coded with the quaternary system. b) The message is coded using nanorods with three different lengths L = 110, 130, or 170 nm and four different orientations <1, <2, <3, and <4 within the unit cell. Depending on the illumination-detection polarizations, different colors—corresponding to different digits within the quaternary system—are observed. c) The 24 digits composing the secret message correspond to 24 nanostructures. d) These 24 nanostructures produce the sequence of colors that corresponds to the secret message only when they are illuminated with the correct polarizations. e–i) Any other polarization combination produces a garbage message.

arbitrary, $R_{\mathrm{H}}^{\mathrm{H}}$, $R_{\mathrm{V}}^{\mathrm{V}}$, and $R_{\mathrm{D}}^{\mathrm{D}}$ share the color bases; $R_{\mathrm{A}}^{\mathrm{D}}$ is independent from other keys; $R_{\mathrm{R}}^{\mathrm{D}}$, and $R_{\mathrm{L}}^{\mathrm{D}}$ have the same colors. By applying nanorods possessing high color contrast with orientations, colors read by different keys become multiple. Such approach increases significantly the options to encrypt the digits as a function of nanorod lengths and rotation angles. In the following demonstration, three nanorod lengths (L = 110, 130, and 170 nm) with four orientation angles within the unite cell (<1: 0°, <2: 45°, <3: 90°, and <4: 135°) are used. In Figure 5b, each structure exhibits different colors under each polarization pairs (keys) of illumination and detection. Yellow colors are labeled as 0, muted colors are assigned as 1, while the remaining distinguishable colors are given 2 and 3 for each polarization pairs, which is compatible with the quaternary coding system. Note that for each polarization pairs, each number can be realized with more than one structure, Figure 5b. This provides additional freedom to choose the encrypted structure.

A possible collection of nanostructures with the key illumination-D detection-D is described in Figure 5c for the plain text “Hello!.” When decrypted with different keys, different color combinations are observed and the concealed information is successfully decrypted only with the correct key, as shown in Figure 5d; applying other keys leads to scrambled messages (Figure 5e to g, note that we have used here the extended ASCII table that includes 256 characters and sequences such as DC2, EOT, ACK, and DC1, which have been underlined to emphasize that they correspond to one single ASCII code). Unlike the binary system, for which an inverted decoding can break the encryption by switching 0 to 1 and vice versa, the quaternary system is very robust and only incorrect messages are produced with the incorrect key, as illustrated in Figure 5h,i.

4. Conclusion

We have described in detail the response of simple plasmonic nanorods to the illumination polarization. Depending on the orientation of that polarization with respect to the symmetry axes of the nanostructure, a chiral response can occur, with the creation of additional field components that were not present in the illumination field. By analyzing this reflected light through a second polarizer, it is possible to control the spectral response of the system at the resolution beyond 80 000 dots per inch (see Section S10, Supporting Information). Specifically, for the Ag nanorods fabricated here, a broad variety of colors can be produced that cover 50% of the chromaticity diagram (see Section S11, Supporting Information). Depending on the illumination and detection polarizations, these colors range from white to vivid colors or even black, in spite of the fact that the material at hand does not absorb much light. Two additional degrees of freedom have been exploited: the nanorod length, which tunes its spectral response, and the nanorod orientation within the unit cell, which modifies the geometrical relationship between the nanorod and the polarization. These different degrees of freedom provide a very rich palette of optical effects that are controlled by the polarization of light. Their utilization to reproduce artworks has been demonstrated, together with their operation as encrypting system, where the polarizations are used as keys and the message is encrypted in a quaternary color subset. The diversity of degrees of freedom provided by this system can enable a wealth of applications in solid-state colors, high-density optical data storage and encryption. The polarization-controlled spectral responses demonstrated in this work could be further extended with freeform and unconventional metaoptics[29] and the assistance of artificial intelligence.[30]

5. Experimental Section

Simulations: Comsol Multiphysics vers. 5.6 was used for numerical simulations. Multiple ports were added as detectors for different polarization states. Periodic boundaries and perfect match layers were applied. The refractive index are plotted in Section S2, Supporting Information.

Fabrication: The samples were fabricated by thin film deposition after electron beam lithography without lift-off or ion-beam etching.[31] Negative resist was used as a spacer, separating the plasmonic structure patterned by E-beam and its complementary-shaped reflector. The steps are as follows: a) A silicon wafer (100/P/SS/01-100) was first baked on a hot plate for 5 min at a temperature of 180 °C to dehydrate it (humidity appears detrimental to nanofabrication[32]). b) Negative tone electron beam photoresist hydrogen silsesquioxane (HSQ, XR-1541-006 DuPont) was then spin-coated on top at 6000 rpm. c) Electron beam exposure with Vistec EBPG5000 system (100 keV and 100 pA). d) Development with Tetra Methyl Ammonium Hydroxide 25% (Honeywell) by immersing the sample for 1 min and then rinsed with DI water and dry with nitrogen for cleaning the toxic chemicals. e) The sample was complete after thin film deposition of 40 nm-thick Ag by Leybold Optics LAB 600H.[32,33]

Optical Measurements: Schematic of the measurement setup shown, in Figure 3a, was implemented on an inverted microscope (Olympus, IX73) operating in reflection mode illuminated with a halogen lamp. Polarized light was achieved by a linear polarizer (Thorlabs, WP25M-UB) and a quarter wave plate (Thorlabs, SAQWP05M-700) in the illumination path (black dashed line) and analyzed also by a quarter wave plate (Thorlabs, SAQWP05M-700) and then a linear polarizer (Thorlabs, WP25M-UB) in the detection path (red dashed line). Cubic beam splitter (Thorlabs, BS022) and an objective (LUCPLFLN 60X, NA = 0.7) operating in air were used. Optical images were taken by a camera (Flir, CM3-U3-50S5C-CS). Reflectance spectra are measured by a spectrometer (Andor Shamrock 303i and Andor Newton 971 EM-CCD). An Ag mirror served as reference. Additional details on the optical setup and the spectral correction can be found in the previous work.[34]

Supporting Information

Supporting Information is available from the Wiley Online Library or from the author.

Acknowledgements

The authors acknowledge the funding provided by the Swiss National Science Foundation (projects 200 021_162 453) and European Research Council (ERC-2015-AdG-695206).

Open access funding provided by Ecole Polytechnique Federale de Lausanne.

Conflict of Interest

The authors declare no conflict of interest.

Data Availability Statement

The data that support the findings of this study are openly available in Zenodo at https://doi.org/10.5281/zenodo.7077502.

Keywords

desaturated colors, encryption, muted colors, plasmonics, polarization, structural colors, vivid colors

Received: September 15, 2022
Revised: November 25, 2022
Published online:

[1] a) A. Kristensen, J. K. W. Yang, S. I. Bozhevolnyi, S. Link, P. Nordlander, N. J. Halas, N. A. Mortensen, *Nat. Rev. Mater.* **2016**, *2*, 16088; b) T. Lee, J. Jang, H. Jeong, J. Rho, *Nano Converg.* **2018**, *5*, 1; c) M. Song, D. Wang, S. Peana, S. Choudhury, P. Nyga, Z. A. Kudyshev, H. Yu, A. Boltasseva, V. M. Shalaev, A. V. Kildishev, *Appl. Phys. Rev.* **2019**, *6*, 041308; d) S. D. Rezaei, Z. Dong, J. Y. E. Chan, J. Trisno, R. J. H. Ng, Q. Ruan, C.-W. Qiu, N. A. Mortensen, J. K. W. Yang, *ACS Photonics* **2021**, *8*, 18; e) Z. Xuan, J. Li, Q. Liu, F. Yi, S. Wang, W. Lu, *The Innovation* **2021**, *2*, 100081.

[2] a) J. Olson, A. Manjavacas, T. Basu, D. Huang, A. E. Schlather, B. Zheng, N. J. Halas, P. Nordlander, S. Link, *ACS Nano* **2016**, *10*, 1108; b) L. Wen, Q. Chen, X. Hu, H. Wang, L. Jin, Q. Su, *ACS Nano* **2016**, *10*, 11076; c) Y. Lee, M.-K. Park, S. Kim, J. H. Shin, C. Moon, J. Y. Hwang, J.-C. Choi, H. Park, H.-R. Kim, J. E. Jang, *ACS Photonics* **2017**, *4*, 1954; d) M. L. Tseng, J. Yang, M. Semmlinger, C. Zhang, P. Nordlander, N. J. Halas, *Nano Lett.* **2017**, *17*, 6034.

[3] J. Zhao, X. Yu, K. Zhou, W. Zhang, W. Yuan, Y. Yu, *Opt. Lasers Eng.* **2021**, *138*, 106421.

[4] Z. Li, Q. Dai, L. Deng, G. Zheng, G. Li, *Opt. Lett.* **2021**, *46*, 480.

[5] J. Cai, C. Zhang, W.-D. Li, *Adv. Opt. Mater.* **2021**, *9*, 2001401.
[6] a) W. Wang, D. Rosenmann, D. A. Czaplewski, X. Yang, J. Gao, *Opt. Express* **2017**, *25*, 20454; b) M. Song, X. Li, M. Pu, Y. Guo, K. Liu, H. Yu, X. Ma, X. Luo, *Nanophotonics* **2018**, *7*, 323; c) L. Cheng, J. Mao, K. Wang, J. Lu, K. Huang, Y. Zhang, L. Zhang, *J. Opt. Soc. Am. B* **2019**, *36*, 3168; d) E. G. Melo, A. L. A. Ribeiro, R. S. Benevides, A. A. G. V. Zuben, M. V. P. dos Santos, A. A. Silva, G. S. Wiederhecker, T. P. M. Alegre, *ACS Appl. Nano Mater.* **2020**, *3*, 1111.
[7] a) E. Schonbrun, G. Möller, G. Di Caprio, *Opt. Lett.* **2014**, *39*, 1433; b) L. Duempelmann, D. Casari, A. Luu-Dinh, B. Gallinet, L. Novotny, *ACS Nano* **2015**, *9*, 12383; c) V. R. Shrestha, S.-S. Lee, E.-S. Kim, D.-Y. Choi, *Sci. Rep.* **2015**, *5*, 12450; d) L. Duempelmann, A. Luu-Dinh, B. Gallinet, L. Novotny, *ACS Photonics* **2016**, *3*, 190; e) I. Koirala, V. R. Shrestha, C.-S. Park, S.-S. Lee, D.-Y. Choi, *Sci. Rep.* **2017**, *7*, 40073; f) Y. Kim, K. Jung, J. Cho, J. K. Hyun, *ACS Nano* **2019**, *13*, 10717; g) J. S. Lee, J. Y. Park, Y. H. Kim, S. Jeon, O. Ouellette, E. H. Sargent, D. H. Kim, J. K. Hyun, *Nat. Commun.* **2019**, *10*, 4782; h) S. Mader, O. J. F. Martin, *Adv. Photonics Res.* **2021**, *3*, 2100245.
[8] a) H. A. Macleod, *Thin-Film Optical Filters*, CRC Press, Boca Raton, FL **2018**; b) S. Mader, O. J. F. Martin, *Light: Adv. Manuf.* **2021**, *2*, 385.
[9] a) K. Kumar, H. Duan, R. S. Hegde, S. C. W. Koh, J. N. Wei, J. K. W. Yang, *Nat. Nano* **2012**, *7*, 557; b) A. S. Roberts, A. Pors, O. Albrektsen, S. I. Bozhevolnyi, *Nano Lett.* **2014**, *14*, 783; c) S. J. Tan, L. Zhang, D. Zhu, X. M. Goh, Y. M. Wang, K. Kumar, C.-W. Qiu, J. K. W. Yang, *Nano Lett.* **2014**, *14*, 4023; d) F. Cheng, J. Gao, T. S. Luk, X. Yang, *Sci. Rep.* **2015**, *5*, 11045; e) M. Miyata, H. Hatada, J. Takahara, *Nano Lett.* **2016**, *16*, 3166; f) V. Flauraud, M. Reyes, R. Paniagua-Domínguez, A. I. Kuznetsov, J. Brugger, *ACS Photonics* **2017**, *4*, 1913; g) R. Mudachathi, T. Tanaka, *Sci. Rep.* **2017**, *7*, 1199; h) H. Wang, X. Wang, C. Yan, H. Zhao, J. Zhang, C. Santschi, O. J. F. Martin, *ACS Nano* **2017**, *11*, 4419; i) B. Yang, W. Liu, Z. Li, H. Cheng, D.-Y. Choi, S. Chen, J. Tian, *Nano Lett.* **2019**, *19*, 4221; j) X. Liu, Z. Huang, J. Zang, *Nano Lett.* **2020**, *20*, 8739; k) W. Yang, S. Xiao, Q. Song, Y. Liu, Y. Wu, S. Wang, J. Yu, J. Han, D.-P. Tsai, *Nat. Commun.* **2020**, *11*, 1864; l) L. Li, J. Niu, X. Shang, S. Chen, C. Lu, Y. Zhang, L. Shi, *ACS Appl. Mater. Interfaces* **2021**, *13*, 4364; m) P. Huo, M. Song, W. Zhu, C. Zhang, L. Chen, H. J. Lezec, Y. Lu, A. Agrawal, T. Xu, *Optica* **2020**, *7*, 1171; n) M. Jiang, S. Y. Siew, J. Y. E. Chan, J. Deng, Q. Y. S. Wu, L. Jin, J. K. W. Yang, J. Teng, A. Danner, C.-W. Qiu, *Mater. Today* **2020**, *35*, 99.
[10] a) Y. Liu, H. Wang, J. Ho, R. C. Ng, R. J. H. Ng, V. H. Hall-Chen, E. H. H. Koay, Z. Dong, H. Liu, C.-W. Qiu, J. R. Greer, J. K. W. Yang, *Nat. Commun.* **2019**, *10*, 4340; b) A. S. Roberts, S. M. Novikov, Y. Yang, Y. Chen, S. Boroviks, J. Beermann, N. A. Mortensen, S. I. Bozhevolnyi, *ACS Nano* **2019**, *13*, 71; c) C. Liu, S. A. Maier, G. Li, *ACS Photonics* **2020**, *7*, 1716; d) A. Weissman, M. Galanty, D. Gachet, E. Segal, O. Shavit, A. Salomon, *Adv. Opt. Mater.* **2017**, *5*, 1700097; e) C. U. Hail, G. Schnoering, M. Damak, D. Poulikakos, H. Eghlidi, *ACS Nano* **2020**, *14*, 1783; f) L. V. Poulikakos, M. Lawrence, D. R. Barton, S. S. Jeffrey, J. A. Dionne, *ACS Photonics* **2020**, *7*, 3216.
[11] a) Y. Nagasaki, M. Suzuki, J. Takahara, *Nano Lett.* **2017**, *17*, 7500; b) E. Panchenko, L. Wesemann, D. E. Gómez, T. D. James, T. J. Davis, A. Roberts, *Adv. Opt. Mater.* **2019**, *7*, 1900893; c) M. Song, Z. A. Kudyshev, H. Yu, A. Boltasseva, V. M. Shalaev, A. V. Kildishev, *Opt. Mater. Express* **2019**, *9*, 779; d) X. Wang, D. Xu, B. Jaquet, Y. Yang, J. Wang, H. Huang, Y. Chen, C. Gerhard, K. Zhang, *ACS Nano* **2020**, *14*, 16832; e) T. D. James, P. Mulvaney, A. Roberts, *Nano Lett.* **2016**, *16*, 3817.
[12] a) T. Ellenbogen, K. Seo, K. B. Crozier, *Nano Lett.* **2012**, *12*, 1026; b) Z. Li, A. W. Clark, J. M. Cooper, *ACS Nano* **2016**, *10*, 492; c) E. Heydari, J. R. Sperling, S. L. Neale, A. W. Clark, *Adv. Funct. Mater.* **2017**, *27*, 1701866; d) V. Vashistha, G. Vaidya, P. Gruszecki, A. E. Serebryannikov, M. Krawczyk, *Sci. Rep.* **2017**, *7*, 8092.
[13] a) X. M. Goh, Y. Zheng, S. J. Tan, L. Zhang, K. Kumar, C.-W. Qiu, J. K. W. Yang, *Nat. Commun.* **2014**, *5*, 5361; b) B. Yang, W. Liu, Z. Li, H. Cheng, S. Chen, J. Tian, *Adv. Opt. Mater.* **2018**, *6*, 1701009.
[14] in *Generalized Phase Contrast*, (Eds: J. Glückstad, D. Palima), Springer Netherlands, Dordrecht **2009**.
[15] a) G. Qu, W. Yang, Q. Song, Y. Liu, C.-W. Qiu, J. Han, D.-P. Tsai, S. Xiao, *Nat. Commun.* **2020**, *11*, 5484; b) X. Li, R. Zhao, Q. Wei, G. Geng, J. Li, S. Zhang, L. Huang, Y. Wang, *Adv. Funct. Mater.* **2021**, *31*, 2103326; c) P. Georgi, Q. Wei, B. Sain, C. Schlickriede, Y. Wang, L. Huang, T. Zentgraf, *Sci. Adv.* **2021**, *7*, eabf9718.
[16] H. Ren, X. Fang, J. Jang, J. Bürger, J. Rho, S. A. Maier, *Nat. Nanotechnol.* **2020**, *15*, 948.
[17] a) Z. Li, C. Chen, Z. Guan, J. Tao, S. Chang, Q. Dai, Y. Xiao, Y. Cui, Y. Wang, S. Yu, G. Zheng, S. Zhang, *Laser Photonics Rev.* **2020**, *14*, 2000032; b) C. Liang, L. Deng, Q. Dai, Z. Li, G. Zheng, Z. Guan, G. Li, *Opt. Express* **2021**, *29*, 10737; c) Q. Dai, Z. Guan, S. Chang, L. Deng, J. Tao, Z. Li, Z. Li, S. Yu, G. Zheng, S. Zhang, *Adv. Funct. Mater.* **2020**, *30*, 2003990; d) P. C. Wu, W.-Y. Tsai, W. T. Chen, Y.-W. Huang, T.-Y. Chen, J.-W. Chen, C. Y. Liao, C. H. Chu, G. Sun, D. P. Tsai, *Nano Lett.* **2017**, *17*, 445; e) F. Ding, B. Chang, Q. Wei, L. Huang, X. Guan, S. I. Bozhevolnyi, *Laser Photonics Rev.* **2020**, *14*, 2000116; f) M. Liu, P. Huo, W. Zhu, C. Zhang, S. Zhang, M. Song, S. Zhang, Q. Zhou, L. Chen, H. J. Lezec, A. Agrawal, Y. Lu, T. Xu, *Nat. Commun.* **2021**, *12*, 2230; g) A. C. Overvig, S. Shrestha, S. C. Malek, M. Lu, A. Stein, C. Zheng, N. Yu, *Light: Sci. Appl.* **2019**, *8*, 92; h) X. Guo, J. Zhong, B. Li, S. Qi, Y. Li, P. Li, D. Wen, S. Liu, B. Wei, J. Zhao, *Adv. Mater.* **2022**, *34*, 2103192.
[18] a) J. Jang, H. Jeong, G. Hu, C.-W. Qiu, K. T. Nam, J. Rho, *Adv. Opt. Mater.* **2019**, *7*, 1970016; b) M. Abdolahi, H. Jiang, B. Kaminska, *Nanotechnology* **2019**, *30*, 405301; c) X. Luo, Y. Hu, X. Li, Y. Jiang, Y. Wang, P. Dai, Q. Liu, Z. Shu, H. Duan, *Adv. Opt. Mater.* **2020**, *8*, 1902020; d) I. Kim, J. Jang, G. Kim, J. Lee, T. Badloe, J. Mun, J. Rho, *Nat. Commun.* **2021**, *12*, 3614.
[19] a) Q. Dai, N. Zhou, L. Deng, J. Deng, Z. Li, G. Zheng, *Phys. Rev. Appl.* **2020**, *14*, 034002; b) L. Deng, J. Deng, Z. Guan, J. Tao, Y. Chen, Y. Yang, D. Zhang, J. Tang, Z. Li, Z. Li, S. Yu, G. Zheng, H. Xu, C.-W. Qiu, S. Zhang, *Light: Sci. Appl.* **2020**, *9*, 101; c) Z. Li, R. Ren, J. Deng, L. Deng, G. Li, G. Zheng, *Opt. Express* **2021**, *29*, 134; d) P. Zheng, Q. Dai, Z. Li, Z. Ye, J. Xiong, H.-C. Liu, G. Zheng, S. Zhang, *Sci. Adv.* **2021**, *7*, eabg0363; e) M. Song, D. Wang, Z. A. Kudyshev, Y. Xuan, Z. Wang, A. Boltasseva, V. M. Shalaev, A. V. Kildishev, *Laser Photonics Rev.* **2021**, *15*, 2000343; f) R. Ren, Z. Li, L. Deng, X. Shan, Q. Dai, Z. Guan, G. Zheng, S. Yu, *Nanophotonics* **2021**, *10*, 2903.
[20] X. Wang, C. Santschi, O. J. F. Martin, *Small* **2017**, *13*, 1700044.
[21] F. J. G. de Abajo, *Rev. Mod. Phys.* **2007**, *79*, 1267.
[22] J. S. Clausen, E. Højlund-Nielsen, A. B. Christiansen, S. Yazdi, M. Grajower, H. Taha, U. Levy, A. Kristensen, N. A. Mortensen, *Nano Lett.* **2014**, *14*, 4499.
[23] a) S. Choi, H. Son, B. Lee, *Opt. Express* **2021**, *29*, 41258; b) M. Hentschel, M. Schäferling, X. Duan, H. Giessen, N. Liu, *Sci. Adv.* **2017**, *3*, e1602735; c) E. S. A. Goerlitzer, A. S. Puri, J. J. Moses, L. V. Poulikakos, N. Vogel, *Adv. Opt. Mater.* **2021**, *9*, 2100378; d) E. Ashalley, K. Acheampong, L. V. Besteiro, P. Yu, A. Neogi, A. O. Govorov, Z. M. Wang, *Photonics Res.* **2020**, *8*, 1213.
[24] H. Okamoto, *J. Mater. Chem. C* **2019**, *7*, 14771.
[25] P. R. West, S. Ishii, G. V. Naik, N. K. Emani, V. M. Shalaev, A. Boltasseva, *Laser Photonics Rev.* **2010**, *4*, 795.
[26] S. Westland, C. Ripamonti, *Computational Colour Science Using MATLAB*, Wiley, Hoboken, NJ **2004**.
[27] H. J. Park, K. B. Kim, E. Y. Cha, *Comput. Intell. Neurosci.* **2016**, *2016*, 5302957.
[28] B. S. Tice, *Proc. SPIE* **2008**, *7075*, 70750Q.
[29] Y. Fan, H. Liang, J. Li, D. P. Tsai, S. Zhang, *ACS Photonics* **2022**, *9*, 2872.

[30] a) A.-P. Blanchard-Dionne, O. J. F. Martin, *Opt. Lett.* **2020**, *45*, 2922; b) M. K. Chen, X. Liu, Y. Sun, D. P. Tsai, *Chem. Rev.* **2022**, *122*, 15356.
[31] B. Abasahl, C. Santschi, T. V. Raziman, O. J. F. Martin, *Nanotechnology* **2021**, *32*, 475202.
[32] X. Wang, C. Santschi, O. J. F. Martin, *Small* **2017**, *13*, 1700044.
[33] K. Thyagarajan, C. Santschi, P. Langlet, O. J. F. Martin, *Adv. Opt. Mater.* **2016**, *4*, 871.
[34] H.-C. Wang, O. J. F. Martin, *Appl. Opt.* **2022**, *61*, 8100.